This is a preprint, the final version is subject to change, of the American Mineralogist (MSA)
Cite as Authors (Year) Title. American Mineralogist, in press.
DOI: https://doi.org/10.2138/am-2019-7076

REVISION 1

COMPOSITE MATERIALS BASED ON ZEOLITE STILBITE FROM FAROE ISLANDS FOR THE REMOVAL OF FLUORIDE FROM DRINKING WATER

ISABEL DÍAZ, LUIS GÓMEZ-HORTIGÜELA, PILAR GÁLVEZ, JOAQUÍN PÉREZ PARIENTE*

Instituto de Catálisis y Petroleoquímica (ICP-CSIC), Marie Curie 2, Cantoblanco, Madrid, Spain.*E-mail: jperez@icp.csic.es

JANA ÓLAVSDÓTTIR

Jarðfeingi (Faroese Geological Survey), Jóannesar Paturssonargøta 32-34, Postbox 3059, FO-110 Tórshavn, Faroe Islands. E-mail: jo@jf.fo

ABSTRACT

In this work, three samples of zeolite stilbite coming from Faroe Islands have been used to prepare zeolite/hydroxyapatite composite materials that have been tested for the removal of fluoride present as geogenic contaminant in underground water. Faroe Islands are an archipelago in the North Atlantic. which have volcanic origins of Paleocene and early Eocene age. Early reports on the presence of zeolites in the Faroe Islands indicate abundance of chabazite, analcite, mesolite, heulandite and stilbite, being heulandite and stilbite dominant in the northern and northwestern part of the islands. Further investigations

of the Faroese Geological Survey have yielded zeolitic phases in Vestmanna, Streymoy, in Morkranes, Eysturoy, as well as in the sea tunnel that connects the island of Eysturoy with island of Borðoy. Three stilbite samples coming from these locations have been used with the aim of producing composite materials for fluoride removal. For this purpose, the samples were contacted with a phosphate solution at room temperature for selected periods of time, in such a way that a hydroxyapatite layer develops on the surface of the zeolite crystals. The resulting composites consist of approximately 93% of zeolite and 7% of nano-hydroxyapatite, which is the active phase for fluoride removal. Excess of fluoride (above 1.5 mg/L according to WHO) in drinking waters provokes dental or skeletal fluorosis, an endemic health problem in more than 25 countries. The defluoridation studies in our work are performed using real waters from Spain with initial [F^-] of 7.1 mg/L. The capacity of the Faroe Islands stilbite-based adsorbent reaches 0.3 mg F^-/g, showing similar behavior regardless of the stilbite sample used. The impact of the particle size of stilbite in the final defluoridation capacity is remarkable. An increase in the particle size leads to a dramatic decrease in the surface area, affecting the growth of the nano-hydroxyapatite on the zeolite surface, hindering as a result its capacity to remove fluoride. Interestingly, electron microscopy and X-ray powder diffraction results clearly show that nano-hydroxyapatite grow on the zeolite surface with a preferential orientation which maximizes the exposition of the (001) face containing the active sites for defluoridation, thus explaining the high F-removal efficiency of these materials.

Keywords: natural zeolite, stilbite, hydroxyapatite, defluoridation

This is a preprint, the final version is subject to change, of the American Mineralogist (MSA)
Cite as Authors (Year) Title. American Mineralogist, in press.
DOI: https://doi.org/10.2138/am-2019-7076

INTRODUCTION

The occurrence of fluoride in excessively high concentration in ground water used for human consumption is a matter of great concern by health care organizations all over the world (Chinoy et al. 1991). The reason for this preoccupation resides in the capacity of this anion to accumulate on teeth and bones, producing an irreversible illness known as fluorosis, a strong deterioration of their functionalities that could ultimately lead, in the most severe cases and in addition to the suffering associated to the illness, to disabling people from normal life. Moreover, not only hard but also soft tissues are targeted by fluoride (WHO 1996). For these reasons, the World Health Organization (WHO) estimated in 1984 that at least 260 million people would be at risk of being affected by this illness due to their consumption of water with a concentration of fluoride higher than 1 mg/L (WHO 1984, UNICEF); as a consequence, WHO strongly recommends the reduction of the concentration of this anion in drinking water below 1.5 mg/L (Fawell 2006). The fluoride present in ground water comes from the leaching of fluoride-rich minerals, mainly fluorite (Ca_2F), criolite (Na_3AlF_6) and hydroxyapatite ($Ca_5(PO_4)_3F$), and there is no way to mitigate the occurrence of this natural dissolution phenomenon (Eawag 2015). Therefore, two alternatives have been envisaged to avoid population exposure to excessive ingestion of this harmful anion. The use of alternative fluoride-free water resources looks at first sight the best action to take, but it is not so much if one considers that in most cases extensive areas are affected by this problem, particularly in developing countries in which the supply of

fresh water coming from distant sources (piped water) is beyond their funding capabilities. The problem is getting worse as in many cases the population is scattered in little villages covering large areas.

For these reasons, efforts have been focused on ex-situ removal of fluoride present in ground water by using a variety of procedures. Current defluoridation technologies can be classified in four distinct groups: precipitation-flocculation, membrane processes, ion exchange and adsorption (Jagtap et al. 2012). To these methods, distillation should also be added (Feenstra et al. 2007). Among these procedures, particular attention is being paid to adsorption technologies, because they do not require additional input energy other than that required for pumping underground water from wells and boreholes, which is always needed, as well as because of their feasible implementation, low operational and maintenance costs, and the possibility to reuse the exhausted adsorbent (Loganathan 2013). However, the energy required to prepare the adsorbent should also be taken into account for a more complete energy balance of the whole process. The key aspect for a successful implementation of defluoridation adsorption technologies resides in the proper choice of the adsorbent. A large variety of different materials have been explored on this regard, including activated alumina, calcium-rich compounds, metal oxides, clays and other soil materials, silica and carbon-based solids, bone char, biopolymers and zeolites (Jagtap et al. 2012). Despite their potential capabilities, many of them experience severe limitations that prevent them for being an adsorbent of choice. In many cases they are not able to meet the WHO recommendation when coping with actual drinking water, which is rich in salts and slightly alkaline, or they release harmful elements under these conditions, as it is often the case with alumina adsorbents (WHO maximum allowable concentration for Al is 0.2 ppm)

(Mulugeta et al. 2014). Zeolites are typically cation exchangers, but they have nevertheless been studied as fluoride adsorbents based upon their large concentration of accessible cations which could be potential sites for F^- binding (in this case, additional cations should also be incorporated for electroneutrality compliance). For this reason, natural zeolites are mostly used due to their abundance and low cost, and to increase their affinity for fluoride they are generally exchanged with multicharged cations like Al^{3+}, Fe^{3+}, La^{3+}, Zr^{4+} (Onyango et al. 2007, Sun et al. 2011, Velazquez-Peña et al. 2017). Natural stilbite from China treated with Fe^{3+} solutions has been shown to be active for fluoride removal, but the effect is mainly due to extraframework iron compounds deposited on the zeolite (Sun et al. 2011). The defluoridation activity of a sample of stilbite from Ethiopia has been shown to improve by a previous NH_4^+/Ca^{2+} exchange, which has been attributed to the generation of connectivity defects during the repeated ionic exchange treatments (Gómez-Hortigüela et al. 2014). Although these methods contribute to improve the defluoridation performance of natural zeolites, this is still below the requirements for actual implementation. In the search for an adsorbent with high capacity for fluoride removal while being able at the same time to cope with groundwater containing relatively low F^- concentration (typically 3-5 mg/L, which is common for many populations affected by fluorosis), attention has been paid to hydroxyapatite, one the most widely tested adsorbent materials. The stability of fluorohydroxyapatite ($K_{ps} = 3.16 \times 10^{-60}$) is higher than that of its hydroxide counterpart ($K_{ps} = 2.34 \times 10^{-59}$), and in the presence of fluoride this anion replaces isomorphically the hydroxide groups located in the hydroxyapatite structure, thus providing a specific removal mechanism for F^-. Although this is the main mechanism for F^- uptake, it is generally accompanied by surface adsorption and, under acidic pH and very high F^- concentration, eventually also by the precipitation of other F-containing solids (Sternitzker et al. 2011).

According to the mechanism of isomorphous substitution of fluoride by hydroxide, the maximum attainable fluoride capacity of HAp would be 37.8 mg F^- per g of HAp. However, the hydroxide groups in the HAp structure are located in narrow 6-membered channels, which impose severe diffusional limitations on the fluoride-hydroxide exchange process. In order to circumvent this problem, , efforts have been made to decrease the crystal size of HAp, and nano HAp (nHAp) indeed exhibits very high defluoridation capacities (Sundaran et al. 2008, Gao et al. 2009, George et al. 2018), which are nevertheless still at least one order of magnitude smaller than the maximum theoretical capacity. Therefore, it would be desirable to enhance the capacity of synthetic HAp for fluoride removal beyond those limits, but undesirable pressure drops during filtration would increase conversely to the reduction of crystal size to the nano-scale, which would impose an operational limit. In order to harmonize these apparently opposite trends, namely enhanced fluoride uptake of nHAp and low pressure drop, we have recently developed an innovative strategy aiming at combining both properties in a single composite material (Gómez-Hortigüela et al. 2013). For this purpose, we have used the calcium-rich zeolite stilbite as calcium supplier for the controlled growth of nHAp on the surface of the zeolite. This procedure led to composite materials that have average particle size in the submillimeter range (75-105 μm), with the benefit of easy applicability, in which the specific defluoridation capacity of the nHAp can be as high as 9 mg F^- per g of nHAp (Gómez-Hortigüela et al. 2014, Sani et al. 2017), much more efficient than bone char, whose active phase is biological hydroxyapatite (Sani et al. 2016).

These studies on the synthesis of stilbite-nHAp composite materials were performed by using a zeolite specimen coming from Ethiopia, collected in the Hasenghe basalt formation,

Tigrai region, with a Ca content of 5.2 wt% (see Gómez-Hortigüela et al. 2014 for a full characterization). The remarkable defluoridation behavior shown by the corresponding composite material prompted us to explore the behavior of other samples of natural stilbites, as well as the influence of some synthesis parameters on their activity in fluoride removal from actual ground waters and to investigate mechanistic details on the formation of the composite material. We report in this work our findings concerning these issues by using three samples of zeolite stilbite coming from the Faroe Islands.

MATERIALS AND EXPERIMENTAL METHODS

Stilbite samples onshore Faroe Islands

Faroe Islands are volcanic islands in the North Atlantic Ocean (Figure 1a) that are part of the North Atlantic Igneous Province (NAIP). The onshore sequence called the Faroe Islands Basalt Group (FIBG) (Figure 1b and c) has a Palaeocene to early Eocene age (Storey et al. 2007, Waagstein 1988, Waagstein et al. 2002). The known onshore stratigraphy is 6.6 km thick whereof the lowermost ~3.4 km is only accessible from the Lopra 1/1A scientific well (Figure 1c).

The lower part of the Faroe Islands Basalt Group - the Lopra Formation - is dominated by volcaniclastic and hyaloclastic rocks, while the middle and upper part of the group are dominated by basaltic lava flows indicative of an overall terrestrial environment (Berthelsen et al. 1984, Passey et al. 2009, Passey et al. 2007, Rasmussen et al. 1969, Rasmussen 1970). The subaerial sequence is subdivided into six lithological defined formations (Passey 2009). The lithological units are dominated by the basalt lava flows of

Beinissvørð, Malinstindur and Enni formations. Three sedimentary units, the Prestfjall Formation and Hvannhagi Formations situated between the Beinisvørð Formation and the Malinstindur Formation, and the Sneis Formation, which stratigraphically is located above the Malinstindur Formation, separate these three formations (Figure 1c). These sedimentary units were deposited during significant breaks in the eruption of the lava flows (Passey et al. 2007).

The lower part of the onshore volcanic - the Lopra and the Beinisvørð formations - deposited during pre-breakup in Chron 26 and 25 from 61 Ma to around 55.5 Ma from a westerly source area (Waagstein 1988, Waagstein et al. 2002, Storey et al. 2007). While Malinstindur and the Enni formations deposited during syn-breakup, in the middle of Chron 24 from around 55.5 to 54 Ma from a northern source area.

Regarding zeolite zones, the northern and western part of Faroe Islands is dominated by stilbite-heulandite zone (Figure 1b, dashed box) while the southern and eastern part of the isles are dominated by mesolite and thomsonite-chabazite zones, respectively (Jørgensen 2006). The three analysed samples from the Faroe Islands are located in the stilbite-heulandite dominated zone and in addition to that all three samples are placed in Malinstindur Formation (Table 1 and Figure 1b and c).

Samples number 2035 and 5096 (Figure 1b and c) are both collected in connection with tunnel construction of a hydroelectrical plant on Streymoy and a subsea tunnel between Eysturoy and Borðoy, respectively. Sample 2031 (Figure 1b and c) was collected in relation to the mapping of the Faroese geology during 1950´s and 1960´s. The diffraction patterns of these three samples (Figure 2) correspond to the stilbite member of a group of minerals

with the same topology, STI, but different space group and chemical composition: barrerite, sodium-rich, orthorhombic; stellerite, calcium-rich, also orthorhombic, and stilbite, which contains both sodium and calcium, monoclinic (Wise 2013). They can therefore be easily distinguished attending to their chemical composition and X-ray powder diffraction pattern, and in particular to the splitting of the 204 and 20-4 reflections which appears at 23-25 2θ deg and is characteristic of the monoclinic structure of the stilbite member of this group (Passaglia et al. 1978, Wise 2013). 2031 and 5096 are pure stilbite minerals, with monoclinic unit cell (see inset in Figure 2); sample 2035 also contains mainly stilbite, but is accompanied by a minor amount of clinoptilolite (vertical arrows). This is further confirmed by chemical analysis (Table 2), where it can be seen that the Ca/Na ratio is in the range 4.7-2.5 for the three samples, as usual for stilbite minerals. It is interesting to note that this ratio varies in parallel to the Si/Al ratio, i.e. low Ca content is associated to Al-rich frameworks. This is in good agreement with the values of Si/Al = 2.75 and Ca/Na = 2.73 reported by Mortier (1983) for a stilbite sample from the Faroe Islands.

Defluoridation experiments

The samples were crushed and sieved to the following four particle size fractions: < 74 μm, 74-105 μm, 105-590 μm and 590-840 μm. Each zeolite fraction was then contacted at room temperature with a phosphate solution following the experimental conditions described previously (Gómez-Hortigüela 2014), in order to induce the growth of hydroxyapatite as nanoparticles connected to the zeolite surface. In this process, the stilbite supplies the calcium required for HAp growing through a cation exchange. Two different crystallization times (2 hours or 6 hours) between the phosphate solution and the zeolite sample were studied.

For the defluoridation experiments, natural water from the Canary Islands containing 7.3 mg/L of fluoride was used (pH = 9.16; total carbonates (CO_3^{2-}+HCO_3^-) = 1365 ± 26 mg/L) (see Table S1 in the Supporting Information for full composition). Defluoridation experiments were carried out at room temperature (23 ± 2 ^oC), with an adsorbent dose of 10 g/L and a contact time of 20 h under continuous magnetic agitation. The concentration of fluoride in the initial solution and after equilibrium upon the addition of the adsorbent was measured by the Ion Selective Electrode technique with a pH & Ion-meter GLP 22 CRYSON, after addition of a total ion strength adjustment buffer (TISAB III, CRISON). All experiments were repeated in order to test the reproducibility and mean values are reported. The defluoridation capacity (Q_e) was calculated following eq. 1:

$$Q_e = \frac{C_o - C_t}{dose} \qquad \text{Equation 1}$$

where C_o is the initial F^- concentration, C_t is the equilibrium F^- concentration (both in mg F^-/L), and the dose is expressed in g/L. The intrinsic capacity of the HAp component (Q_{HAp}) was determined from Q_e by normalization to the amount of HAp calculated from the P wt% content measured by ICP.

Characterization techniques

Powder X-Ray Diffraction (XRD) patterns were collected with an X'pert Pro PANalytical diffractometer equipped with an X'celerator detector using a Cu K_α radiation and Ni filter, which has a wavelength of 1.54056 Å. The chemical inorganic composition has been determined by Inductively Coupled Plasma Optical Emission Spectrometry (ICP-OES,

Optima 3300 DV model). Surface area was calculated using N_2 in a ASAP2024 Micromeritics. Infrared measurements were carried out using an Attenuated Total Reflectance spectrophotometer (ATR, PIKE TECHNOLOGIES) in the range of 500-4000 cm^{-1}, using quartz as detector. Scanning electron microscopy (SEM) micrographs were collected with a Philips XL30 S-FEG microscope using Cr coating to enhance resolution. Transmission Electron Microscopy was performed using STEM/EDX Mapping mode in a JEOL 2100F operating at 200 kV. Prior to observations, the samples were dispersed in ethanol and placed onto a holey carbon copper micro grid.

RESULTS AND DISCUSSION

Synthesis of the composite materials

An important parameter for designing packed bed systems for fluoride removal from drinking water is the particle size of the adsorbent material, as it might affect the overall performance of the system. For this reason, we have prepared composite nHAp-stilbite materials for each zeolite in the particle size ranges indicated in the experimental section following the procedure referred, and tested their activity in the removal of fluoride from natural water containing 7.3 mg/L of fluoride. Prior works (Gómez-Hortigüela et al. 2014, Sani et al. 2017) have shown the actual formation of HAp in this zeolite-based system in the conditions described in the experimental section. The amount of nHAp present in the material can be monitored from the P content of the sample, while the morphology and crystal size of the nHAp can be assessed by Electron Microscopy. For the sake of simplicity, representative results of the 2031 sample will be presented in this section. Table 3 collects the P content and defluoridation capacity of this sample. It can be seen that the P content is 1.3 wt% for the smallest particle size ($d<74$ μm), but it decreases strongly as the

particle size increases, up to becoming negligible for the 105-590 μm and larger fractions. This result suggests that the nucleation process of the nHAp onto the zeolite surface is strongly controlled by the exchange of the cations of the solution by the Ca^{2+} ions located inside the zeolite channels, and the consequent diffusion of Ca^{2+} to the zeolite external surface and contact the fluid medium thus enabling building up the HAp structure by reacting with the phosphate anions therein present. The cationic exchange process will in this way be strongly influenced by the particle size, and it has been indeed shown that the exchange of Ca^{2+} in stilbite is a slow process (Gómez-Hortigüela et al. 2014, Sani et al. 2017). However, the grinding treatment of the zeolites could also eventually stimulate their ability for the formation of nHAp by generating additional nucleation sites.

Figure 3 shows representative SEM images of the bare zeolite samples, compared with those corresponding to the d<74 μm fraction after formation of the nHAp phase in 6 days of crystallization. At high magnifications it is possible to observe in the stilbite crystals the steps and terraces formed during crystal growth of the zeolite. After contacting with the phosphate solution, the zeolite surface is covered with small crystals of nHAp of hexagonal-plate morphology, which are nearly 1 μm width and around 20 nm thick. These nHAp crystals cover tightly the entire surface, wrapping the steps and terraces therein present. The thickness of the nHAp crystals varies between ~13 nm (in smaller crystals, indicative of the initial stages of crystal growth) and ~24 nm (at the end of the crystal growth). Figure 4 shows the X-ray powder diffraction patterns of the original sample 2031 (line marked with “a”), and those of the composite with an intermediate amount of HAp (line noted as “b”, prepared with the 74-105 μm fraction after 6 days of treatment, which contained 1.6 % of HAp as deduced from the P content), and with a high amount of HAp

(line "c", prepared with the d<74 μm fraction after 6 days of crystallization, with 7.0 % of HAp), where the resistance of the stilbite framework to the treatment is clearly confirmed. The process of crystallization of hydroxyapatite can be monitored by X-ray powder diffraction: on the one hand, the cationic exchange to release Ca^{2+} to the external surface of the zeolite involves a change of symmetry from monoclinic in the original stilbite, which gives the three peaks previously mentioned at ~24 2θ deg (see left inset in Figure 4, line "a"), to orthorhombic in the exchanged composite material, characterized by a single peak (see the evolution upon increase of HAp crystallization, "b" and "c" lines). On the other hand, the progressive formation of HAp in the composite materials can be distinguished by the appearance of a peak at ~32 2θ deg (see right inset in Figure 4), characteristic of the (211) diffraction of HAp (JCPDS card no. 09-0432), which is most intense in the material with the highest amount of HAp (line "c"). Worth is noting the increase of the intensity of the peak at 25.6 2θ upon formation of HAp (dashed arrow), which can be assigned to the (002) diffraction of HAp. In usual non-preferentially oriented HAp crystals, this peak is less intense than that corresponding to (211) (Panda et al. 2003), but when the crystal growth takes place preferentially on the a(b) direction, the c-orientation of the HAp hexagonal plates provoke an enhancement of the (002) diffraction (Chen et al. 2016). Some other minor changes in the X-ray powder diffraction patterns are observed, which might be associated to the cationic exchange and the resulting changes of symmetry, but characteristic assignments could not be made. In sum, SEM and X-ray powder diffraction results point to a preferential growth of nHAp crystals on the a(b) axis, resulting in large (001) crystal surfaces.

Infrared spectroscopy (Figure 5) in the bare STI zeolite (line "a") shows bands around 1000 cm^{-1} due to vibrations of the zeolite network, while the band at 1634 cm^{-1} is assigned to the deformation of adsorbed water molecules. In the composite materials where hydroxyapatite is grown onto the zeolite surface, a new band can clearly be distinguished as a shoulder at ~1020 cm^{-1}, which is consistent with the formation of hydroxyapatite (Kanno 2014). Indeed, the intensity of this band is enhanced upon an increase of the amount of P, which is 0.3% for HAp grown on the 74-105 μm STI particles (line "b"), and 1.3% for the sample obtained with <74 μm STI particles (line "c"), thus confirming the higher formation of HAp in the smaller particles.

Finally, Transmission Electron Microscopy allows identifying the chemical composition while observing the structure at local level. Figure 6 shows a STEM image of the nHAp-STI composite obtained from sample 2013 with d<74 μm particle size, in which the solid profile of the stilbite is observed covered by small thin crystals grown homogeneously all over the surface. Using EDX it is possible to identify the chemical composition of both phases, being the inner solid contrast mainly composed by Si and Al (characteristic of the zeolite), while the outer hairy crystals are formed by P and Ca, coming from hydroxyapatite. These results clearly confirm that nHAp is grown onto the external zeolite surface and keeps adhered to it, hence providing HAp nanoparticles supported on large zeolite particles that are easy to handle.

Defluoridation studies

Once characterized the crystallization of HAp on the zeolite surface of these samples, we finally performed F-removal studies in order to test the defluoridation ability of these

nHAp-STI composite materials. The influence of the particle size of the three zeolite samples on their ability to build up nHAp on the surface is directly reflected on their defluoridation capacity (Figure 7). For the three samples, high defluoridation values are found for the smallest particle size (d<74 μm), in the range 0.40-0.44 mg F^-/g, but the capacity decreases rapidly for bigger particles, being the largest size (590-840 μm) nearly inactive. This behaviour is a clear indication that the formation of the active nHAp phase on the surface of the samples is a slow, diffusion-controlled process, as it is evidenced by the lower capacity of the composite material synthesized with 2 days of crystallization time, compared with that of 6 days (Table 4). This is a general behaviour of the three samples, and it does not depend therefore on their specific origin. However, some differences are observed regarding the capacity of the most active size fraction (d<74 μm), where the defluoridation activity of the samples follows the order 5096 > 2031 > 2035. It could be expected in a first approach that, as Ca is required to build up the nHAP crystals, this order should parallel the Ca content of the stilbite samples. However, this is not the case, because the most active composite material is the one with the lowest Ca content (sample 5096), the order being 2031 (6.9 wt%) > 2035 (6.2 %) > 5096 (6.0 %). Therefore, other factors should account for the observed differences. As the crystallization of nHAp is a surface phenomenon, it could be related in a first instance to the external surface area of the bare stilbite crystals, whose values are reported in Table 2. The external area is low for all three zeolite specimens, in the range 1-5 m^2/g –consistent with their very large crystal size–, but nevertheless they differ significantly. The presence of surface features such as steps and terraces would contribute in a significant manner to the total surface area. The sample with the highest surface area, 5.1 m^2/g, is 5096, the one with the highest defluoridation capacity,

while the surface areas of the 2031 and 2035 samples are much lower and similar, 1.4 m^2/g. These results can provide an explanation for the defluoridation capacities discussed above as follows. For those two samples with the smallest surface area, the crystallization of nHAp, and hence their defluoridation capacity, would be regulated by their Ca content. However, higher surface area would enhance the nucleation of nHAp, compensating in this way the lower Ca content of sample 5096. These two properties of the zeolites, namely Ca content and surface area, are therefore critical in determining their ability to favour the crystallization of nHAp. However, other factors should also be playing a role in the process, as it is evidenced by comparing the defluoridation activity of these samples with that of another stilbite specimen from Ethiopia previously reported (Gómez-Hortigüela et al. 2014, Sani et al. 2017). The Ca content of this material was 5.3 wt%, and its surface area 2.3 m^2/g. Both values are lower than those of the most active stilbite sample reported in this work (5096), but contrary to expectation, its defluoridation capacity is nevertheless higher, 0.46 mF^-/g for the 74-105 μm fraction. This result suggests that the chemical nature of the surface of these two zeolites is different, and that Ca content and surface area are not the only factors to consider to account for the capability of this natural zeolite to trigger the nucleation of nHAp on the stilbite surface under the conditions described in this work. Moreover, it has been reported that a mixture of monoclinic and orthorhombic structures is formed upon NH_4^+ exchange of Ca-stilbite, and in addition connectivity defects are also generated during the exchange process (Gómez-Hortigüela et al. 2014).

Let us have a final discussion about the mechanism of the HAp crystal growth on the stilbite surface. HAp crystallizes in the hexagonal system, and the crystals develop two major crystal planes: the *a* (or *b*) plane, i.e. the (100) face, which is perpendicular to the

*a(b)*axis, and the *c*-plane, (001) face, which is perpendicular to the c-axis of the crystals and therefore perpendicular to the 6-ring narrow tunnels where the columns of hydroxide groups are located in the structure (Figure 8, top-right). The OH^-/F^- exchange that takes place during water defluoridation should imply diffusion of the incoming fluoride anions along these 6-ring channels and the corresponding counter-diffusion of the OH^- ions to the exterior.

A close examination of the composite materials under SEM may provide some clues on the crystallization process. It can be seen in Figure 8 that some areas of the 2035 sample are not fully covered by HAp crystals, which allow us to identify the early stages of the crystal growth process. Very thin nHAp crystals with plate-shape morphology of size 13-24 nanometres thick and 100 nm width are seen to grow highly ordered on the surface, with the *a*-plane adhered on top of the zeolite surface, and the *c*-plane perpendicular to this surface. Therefore, crystal growth along *b*(*a*) axis is strongly favoured over that along *c* axis, leading to the observed thin plate-shape morphology. It has been reported (Aizawa et al. 2013, Okada et al. 2015, Haider et al. 2017) that the *a(b)*-plane (*ac* and *bc* crystal faces) is rich in calcium ions, while the *c*-plane (*ab* crystal face) is rich in phosphate and hydroxide ions. Therefore, the HAp crystals are growing on the surface of the stilbite through the calcium-rich *a(b)*-plane. The framework type of stilbite group consists of two sets of interconnected channels. The 10-membered ring channel runs along the *a*-axis, while the 8-membered channel extends along [001] direction. Therefore, the (010) face is the one with the highest density of framework elements (Si, Al and O) and extraframework cations, most of them calcium ions. Moreover, it has been reported that the stilbite crystals usually develop prominent (010) faces (Wise 2013), which is most probably the one with

the lowest surface energy owing to its densely packed atom arrangement, and it is also a preferred cleavage plane. Taking into account all these considerations, despite the observations of the full coverage of the zeolite crystals, it could be hypothesized that the high density of calcium ions present in the (010) stilbite plane would provide a preferential interface to facilitate the nucleation of the HAp along its calcium-rich *b*-plane through their interaction with the phosphate ions present in the solution. A scheme of such interaction and HAp growing process is depicted in Figure 8.

The defluoridation capacity of the composite material is basically due to their nHAp content. Hence, it is possible to determine the intrinsic capacity of the nHAp component of the composite material based on the P content. This has been done for the two fractions of smaller size of sample 2031 (Table 3, Q_{HAp}). Very high intrinsic capacity is found for the sample with the smallest P content, which corresponds therefore to an early stage of the crystallization of nHAp. For this sample, nearly 1/3 of the total hydroxide groups present in the structure have been replaced by fluoride anions. This very efficient OH^-/F^- exchange process has been made possible by the extremely thinness of the anisotropic nHAp crystals along the *c*-axis, which facilitates the diffusion along the narrow hexagonal tunnel that extends along this direction. For the more advanced stages of the crystallization process, here represented by the d<74 μm fraction with a P content of 1.3 wt%, the intrinsic defluoridation capacity of the nHAp decreases, although it still reaches a remarkable 16% of the total OH^-; this decrease in intrinsic capacity is due to the growth of crystals along the *c*-direction. As previously mentioned, nHAp crystals (of the d<74 μm fraction) display a thickness (along c) of ~20 nm. Taking into consideration that the 'c' unit cell parameter of HAp is 0.688 nm, this involves that our nHAp crystals contain ~29 unit cells along c, of

which only 16% have exchangeable OH- anions, i.e. 4.7 unit cells along c, which corresponds to 2.3 u.c. from each side of the crystal plates. Hence, we can conclude that the active nHAp thickness where hydroxide anions can be exchanged by F^- is 1.6 nm from each side, and therefore nHAp crystals of around 3.2 nm should display maximum defluoridation activity.

IMPLICATIONS

This work demonstrates that stilbite natural zeolites have a strong potential to be used as support for the controlled growth of nanoparticles of hydroxyapatite which are very active for the elimination of fluoride from water, a serious problem in many countries where groundwater with high fluoride concentrations are used as drinking water. The particular origin of the stilbite samples coming from different geological areas provide materials with distinct physico-chemical properties, in particular surface area and Ca content, that strongly affect the performance of the obtained composite materials. Interestingly, the crystal chemistry of stilbite natural zeolites provides a control on the growth of nanoparticles over the zeolite surface with a preferential orientation. In our case, this leads to hydroxyapatite nanoparticles with a maximum exposition of the (001) crystalline face; this is particularly interesting since this is the most active face for defluoridation because it contains the hydroxide active sites for substitution with fluoride. Our work demonstrates that the particular cationic exchange and surface chemistry properties of natural zeolites can be extremely useful to provide a controlled growth of different nanoparticles of targeted materials on their external surface, which has been elaborated here for hydroxyapatite but should be extendable to other active phases as well.

ACKNOWLEDGEMENTS

Luis González from TAGUA S.L. is acknowledged for the contact with the Faroe Geological Survey. This work has been partially financed by the Spanish State Research Agency (Agencia Española de Investigación, AEI) and the European Regional Development Fund (Fondo Europeo de Desarrollo Regional, FEDER) through the Project MAT2016-77496-R (AEI/FEDER, UE). C. Márquez-Álvarez is acknowledged for collecting the infrared spectra.

REFERENCES

Aizawa, M., Matsura, T. and Zhuang, Z. (2013) Synthesis of single-crystal apatite particles with preferred orientation to the a- and c-axes as models of hard tissue and their applications. Biological and Pharmaceutical Bulletin, 36, 1654-1663.

Berthelsen, O., Noe-Nygaard, A., and Rasmussen, J. (1984) The Deep Drilling Project 1980–1981 in the Faeroe Islands: Tórshavn, Føroya Fróðskaparfelag.

Chen, W., Tian, B., Lei, Y., Ke, Q.F., Zhu, Z.A., Guo, Y.P. (2016) Hydroxyapatite coatings with oriented nanoplate and nanorod arrays: Fabrication, morphology, cytocompatibility and osteogenic differentiation. Materials Science and Engineering C67 395-408

Chinoy, N. J., Rao, M. V., Narayana, M. V., Neelakanta, E. (1991) Microdose vasal injection of sodium fluoride in the rat. Reproductive Toxicology. 5, 505 - 512.

Eawag (2015) Geogenic Contamination Handbook – Addressing Arsenic and Fluoride in Drinking Water. C. A. Johnson, A. Bretzler (Eds.), Swiss Federal Institute of Aquatic Science and Technology (Eawag), Dübendorf, Switzerland.

Fawell, J., Bailey, K., Chilton, J., Dahi, E., Fewtrell, L., Magara Y. (2006) Fluoride in Drinking water, World Health Organisation, IWA Publishing, London.

Feenstra, L., Vasak, L., Griffioen, J. (2007) Fluoride in groundwater: Overview and evaluation of removal methods. International Groundwater Resources Assessment Centre (IGRAC), Utrecht, The Netherlands.

Gao, S., Sun, R., Wei, Z., Zhao, H., Li, H., Hu, F. (2009) Size-dependent defluoridation properties of synthetic hydroxyapatite. Journal of Fluorine Chemistry, 130, 550-556.

George, S., Mehta, D., Saharan, V. K. (2018) Application of hydroxyapatite and its modified forms as adsorbents for water defluoridation: an insight into process synthesis. Reviews in Chemical Engineering, published online. DOI: 10.1515/revce-2017-0101

Gómez-Hortigüela, L., Pérez Pariente, J., Díaz Carretero I., Chebude, Y. (2013) Natural zeolite-nanohydroxyapatite compound material, method for preparing same and use thereof for removing fluoride from water. International patent, WO2014131926.

Gómez-Hortigüela, L., Pérez-Pariente, J., Chebude, Y., Díaz I., (2014) Controlled growth of hydroxyapatite on the surface of natural stilbite from Ethiopia: application in mitigation of fluorosis. RSC Advances, 4, 7998-8003.

Gómez-Hortigüela, L., Pinar, A. B., Pérez-Pariente, J. Sani, T., Chebude, Y., and Diaz, I. (2014) Ion exchange in natural zeolite stilbite and significance in defluoridation ability. Microporous and Mesoporous Materials, 193, 93-102.

Haider, A., Haider, S., Han, S. S., and Kang, I-K. (2017) Recent advances in the synthesis, functionalization and biomedical applications of hydroxyapatite: a review. RSC Advances, 7, 7442-7458.

Jagtap, S., Yenkie, M.K., Labhsetwar, N., Rayalu, S. (2012) Fluoride in drinking water and defluoridation of water. Chemical Reviews, 112, 2454-2466.

Kanno, C.M., Sanders, R.L., Flynn, S.M., Lessard, G., Myneni, S.C.B., (2014) Novel apatite-based sorbent for defluoridation: synthesis and sorption characteristics of nano–micro-crystalline hydroxyapatite-coated-limestone. Environmental Science and Technology 48, 5798–5807.

Jørgensen, O. (2006) The regional distribution of zeolites in the basalts of the Faroe Islands and the significance of zeolites as palaeotemperature indicators., *in* Chalmers, J. A., and Waagstein, R., eds., Scientific results from the deepened Lopra-1 borehole, Faroe Islands, Volume 9: Copenhagen, Geological Survey of Denmark and Greenland, p. 123-156.

Loganathan, P., Vigneswaran, S., Kandasamy, J., Naidu, R. (2013) Defluoridation of drinking water using adsorption processes. Journal of Hazardous Materials, 248–249, 1–19.

Mortier, W. (1983) Thermal stability of the stilbite-type framework: crystal structure of the dehydrated sodium/ammonium exchange form. American Mineralogist, 68, 414-419.

Mulugeta, E., Zewge, F., Johnson, C. A., Chandravanshi, B. S. (2014) A high-capacity aluminum hydroxide-based adsorbent for water defluoridation. Desalination and Water Treatment, 52, 5422–5429.

Okada, M., and Matsumoto, T. (2015) Synthesis and modification of apatite nanoparticles for use in dental and medical applications. Japanese Dental Science Review, 51, 85-95.

Panda, R.N., Hsieh, M.F., Chung, R.J., Chin, T.S. (2003) FTIR, XRD, SEM and solid state NMR investigations of carbonate-containing hydroxyapatite nano-particles synthesized by hydroxide-gel technique. Journal of Physics and Chemistry of Solids, 64, 193-199.

Passaglia, E., Galli, E., Leoni, L. (1978) The crystal chemistry of stilbites and stellerites. Bulletin de Minéralogie, 101, 368-375.

Passey, S. R. (2009) Recognition of a faulted basalt lava flow sequence through the correlation of stratigraphic marker units, Skopunarfjørður, Faroe Islands, Tórshavn, Annales Societatis Scientiarum Færoensis. Faroe Islands Exploration Conference: Proceedings of the 2nd Conference, p. 174-204.

Passey, S. R. and Bell, B. R. (2007) Morphologies and emplacement mechanisms of the lava flows of the faroe islands basalt group, faroe islands, NE atlantic ocean: Bulletin of Volcanology, 70, 2, 139-156.

Passey, S. R., and Jolley, D. W. (2009) A revised lithostratigraphic nomenclature for the palaeogene Faroe Islands basalt Group, North Atlantic: Earth and Environmental Science Transaction of the Royal Society of Edinburg, 99, 127-158.

Rasmussen, J., and Noe-Nygaard, A. (1969) Beskrivelse til Geologisk Kort over Færøerne i målestok 1:50.000, København, C. A. Reitzels Forlag (Jørgen Sandal), Geological Survey of Denmark I. Series, 370.

Rasmussen, J. (1970) Geology of the Faroe Islands (Pre-Quaternary). Trans: Henderson G.: Geological Survey of Denmark, Copenhagen, v. (1/25).

Sani, T., Gómez-Hortigüela, L., Pérez-Pariente, J., Chebude, Y., Díaz I. (2016) Defluoridation capacity of nano-Hidroxyapatite/stilbite composite compared with Bone Char. Separation and Purification Technologies, 157, 241-248.

Sani, T., Gómez-Hortigüela, L., Chebude, Y., Díaz, I., Pérez-Pariente J. (2017) Controlled growth of nano-hydroxyapatite on Stilbite: Defluoridation performance. Microporous and Mesoporous Materials 254, 86-95.

Storey, M., Duncan, R. A., Tegner, C. (2007) Timing and duration of volcanism in the North Atlantic Igneous Province: Implications for geodynamics and links to the Iceland hotspot. Chemical Geology, 241(3), 264-281.

Sundaram, C.S., Viswanathan, N., Meenakshi, S. (2008) Defluoridation chemistry of synthetic hydroxyapatite at nano scale: equilibrium and kinetic studies. Journal of Hazardous Materials, 155, 206-215.

UNICEF's Position on Water Fluoridation, <http://www.nofluoride.com/Unicef_fluor.cfm> (consulted on 04.07.19).

Velazquez-Peña, G.C., Olguín-Gutiérrez, M.T., Solache-Ríos, M.J., Fall, C. (2017) Significance of FeZr-modified natural zeolite networks on fluoride removal. Journal of Fluorine Chemistry, 202, 41-53.

Waagstein, R. (1988) Structure, composition and age of the Faeroe basalt plateau. In A. C. Morton and L. M. Parson, Eds., Early Tertiary Volcanism and the Opening of the NE Atlantic, Volume 39, Geological Society, London, Special Publications, p. 225-238.

Waagstein, R., Guise, P., and Rex, D. (2002) K/Ar and $^{39}Ar/^{40}Ar$ whole-rock dating of zeolite facies metamorphosed flood basalts: the upper Paleocene basalts of the Faroe Islands, NE Atlantic. In D. W. Jolley and B. R. Bell, Eds., The North Atlantic Igneous province: Stratigraphy, tectonic, Volcanic and Magmatic Processes, Geological Society of London, p. 219-251.

Wise, W. (2013) Handbook of Natural Zeolites. Edited by Carmine Colella, De Frede Editores, Naples.

WHO (1984) Guidelines for Drinking Water Quality, Recommendations,Vol. 1, World Health Organization, Geneva, Switzerland.

WHO (1996) Guidelines for Drinking Water Quality, Health Criteria and Other Information, second ed., Vol. 2,World Health Organization, Geneva, Switzerland.

Caption to Figures

Figure 1. (A) Regional location map of the study area where the black box in the centre of the map outline the Faroe Islands (B) Geological map of the Faroe Islands referring to the location of the three samples (black circles) analysed in this study. (C) Stratigraphic column of the Faroe Islands Basalt Group (FIBG) and the stratigraphic placement of samples analysed in this study.

Figure 2. X-ray powder diffraction of the three zeolite stilbite samples of the Faroe Islands. Vertical arrows indicate impurities of clinoptilolite.

Figure 3. SEM images of bare zeolite sample 2031 at two magnifications, and the corresponding nHAp-containing composite grown in 6 days with the d<74 μm fraction.

Figure 4. X-ray powder diffraction profiles of (a) zeolite sample 2031; (b) the composite with an intermediate amount of HAp prepared with the 74-105 μm fraction after 6 days of treatment, and (c) the composite material prepared with the d<74 μm fraction in 6 days where the reflections of HAp are marked with arrows.

Figure 5. IR-ATR spectra of of (a) zeolite sample 2031; (b) the composite with an intermediate amount of HAp prepared with the 74-105 μm fraction after 6 days of treatment, and (c) the composite material prepared with the d<74 μm fraction in 6 days where the band of HAp is marked with arrow.

Figure 6. STEM/EDX mapping of the 2031/HAp composite materials prepared with the d<74 μm fraction in 6 days of crystallization.

Figure 7. Defluoridation capacity of the stilbite composite samples as a function of the particle size, for 6 days of HAp crystallization; adsorbent dose: 10 g/L.

Figure 8. Hydroxyapatite SEM image and structure (top). Stilbite/HAp SEM image (sample 2035) and representation of the interaction at the zeolite surface (bottom).

This is a preprint, the final version is subject to change, of the American Mineralogist (MSA)
Cite as Authors (Year) Title. American Mineralogist, in press.
DOI: https://doi.org/10.2138/am-2019-7076

Tables

Table 1. An overview of the stilbite samples analysed in this study.

JF Nr	Mineral	Long. E	Lat. N	Place	Date	Weight (g)
2031*	stilbite	-7,14571	62,164876	Tunnel in Vestmanna	01-01-1953	131.41
2035*	stilbite	-7,09911	62,153487	Heljareyga, Vestmanna	01-07-1961	116.09
5096	stilbite	-6,70572	62,213066	Subsea Tunnel, Norðoyartunnilin	02-02-2005	78.01

*the position of samples 2031 and 2035 is an approximate location.

This is a preprint, the final version is subject to change, of the American Mineralogist (MSA)
Cite as Authors (Year) Title. American Mineralogist, in press.
DOI: https://doi.org/10.2138/am-2019-7076

Table 2. Chemical composition (in wt%) and external surface area of the three stilbite samples.

Sample	**2031**	**2035**	**5096**
$S_{BET}(m^2/g)$	1.5	1.4	5.1
Na	0.85	1.12	1.38
Mg	0.30	0.05	0.07
Ca	6.89	6.17	5.95
Si	31.28	30.77	29.72
Al	9.00	9.90	10.10
Fe	0.33	0.17	1.42
As	0.09	0.12	0.10
Si/Al (mol)	3.3	3.0	2.8
Ca/Na (mol)	4.7	3.2	2.5

This is a preprint, the final version is subject to change, of the American Mineralogist (MSA)
Cite as Authors (Year) Title. American Mineralogist, in press.
DOI: https://doi.org/10.2138/am-2019-7076

Table 3. P content after 6 days of crystallization, calculated HAp wt % determined from P content (in brackets) and defluoridation capacity of different size fractions of sample 2031. The intrinsic defluoridation capacity of the HAp component of the composite material (Q_{HAp}) is also reported. Figures in brackets (in Q_{HAp} column) correspond to the fraction of OH^- present in the HAp crystal structure actually replaced by F^-. Pure fluoroapatite contains 37.8 mg F^-/g.

Fraction (µm)	**S_{BET} (m^2/g)**	**[P] in wt% (HAp wt%)**	**Q_e (mg F^-/g)**	**Q_{HAp} (mg F^-/g)**
<74	1.9	1.3 (7.0)	0.42	6.0 (15.9%)
74-105	1.5	0.3 (1.6)	0.20	12.3 (32.5%)
105-590	0.3	<0.1	0.04	-
590-840	0.1	<0.1	0.00	-

This is a preprint, the final version is subject to change, of the American Mineralogist (MSA)
Cite as Authors (Year) Title. American Mineralogist, in press.
DOI: https://doi.org/10.2138/am-2019-7076

Table 4. Defluoridation capacity of the 74-105 μm fraction as a function of the crystallization time (2 days and 6 days). Adsorbent dose: 10 g/L.

Sample	**Crystallization time**	**Capacity (mg F/g)**
2031	2 d	0.15
	6 d	0.20
2035	2 d	0.16
	6 d	0.20
5096	2 d	0.19
	6 d	0.24

Figure 1

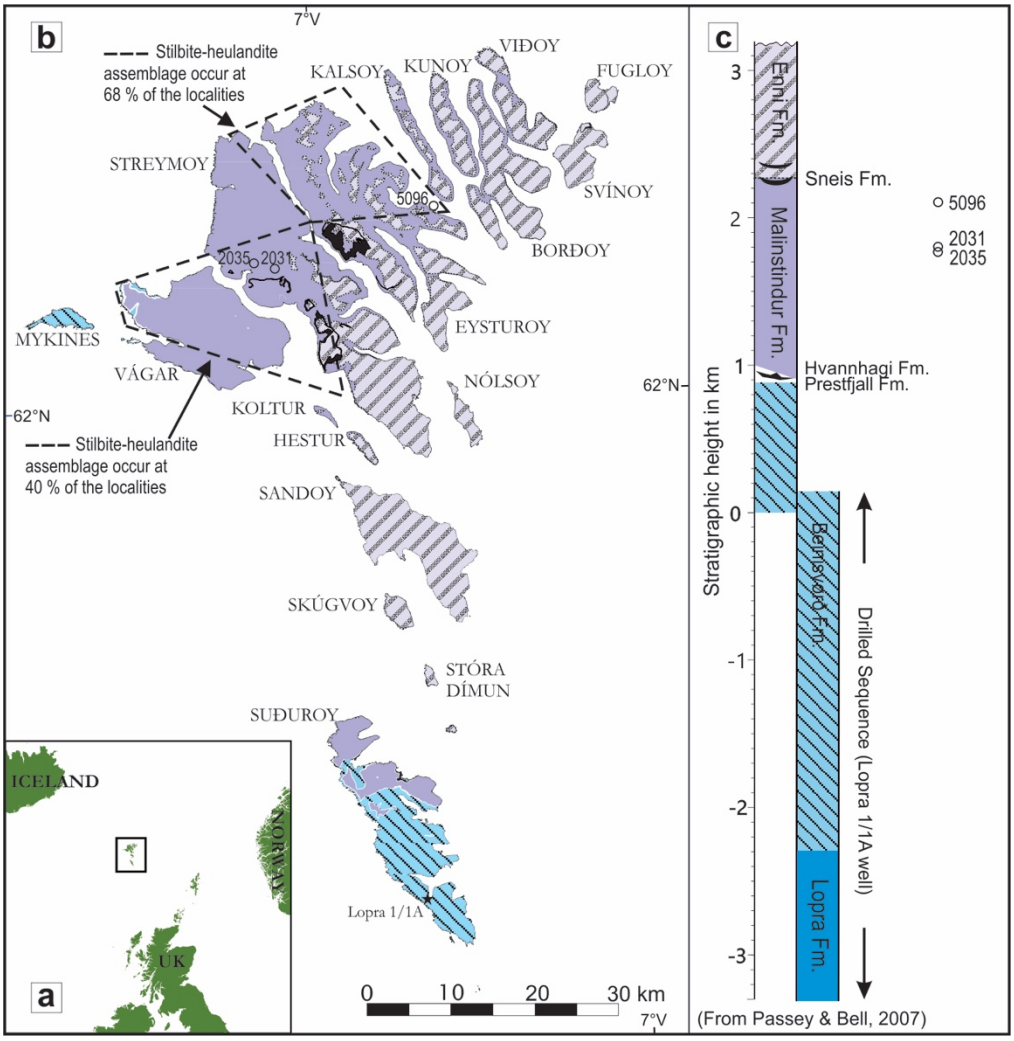
b
7°V
Stilbite-heulandite assemblage occur at 68 % of the localities
KALSOY
KUNOY
VIÐOY
FUGLOY
STREYMOY
SVÍNOY
5096
BORÐOY
2035
2031
EYSTUROY
MYKINES
VÁGAR
NÓLSOY
62°N
KOLTUR
HESTUR
Stilbite-heulandite assemblage occur at 40 % of the localities
SANDOY
SKÚGVOY
STÓRA DÍMUN
SUÐUROY
ICELAND
NORWAY
UK
a
Lopra 1/1A
0 10 20 30 km
7°V
c
Stratigraphic height in km
3
2
1
0
-1
-2
-3
Enni Fm.
Sneis Fm.
Malinstindur Fm.
Hvannhagi Fm.
Prestfjall Fm.
Beinisvord Fm.
Lopra Fm.
5096
2031
2035
Drilled Sequence (Lopra 1/1A well)
(From Passey & Bell, 2007)

Figure 2.

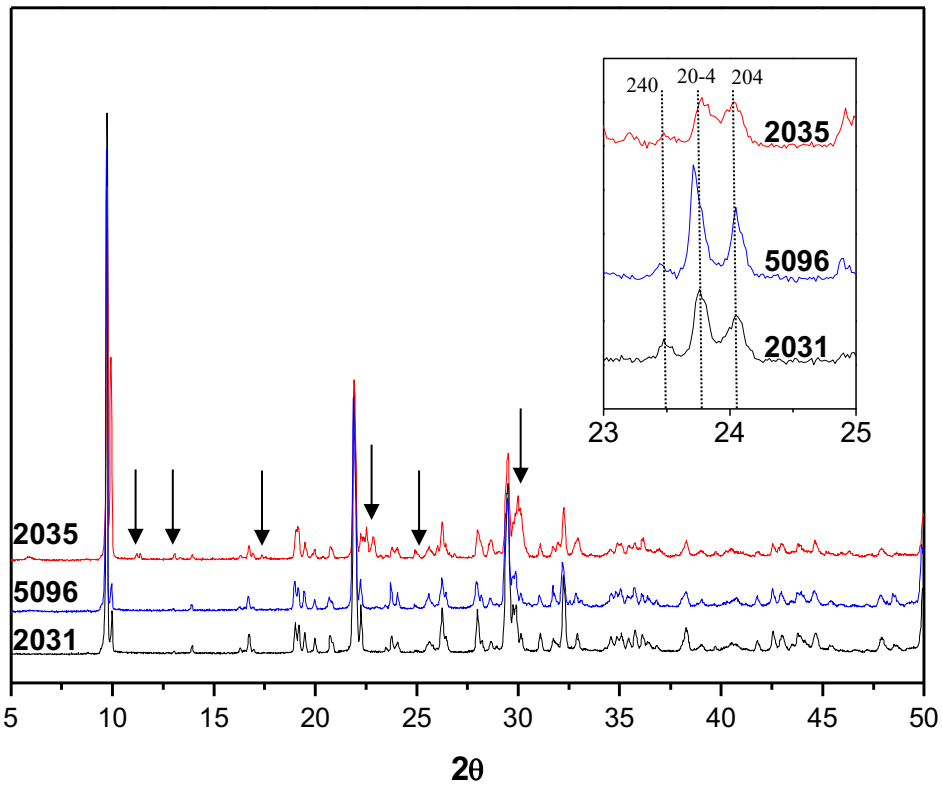
240
20-4
204
2035
5096
2031
23
24
25
2035
5096
2031
5
10
15
20
25
30
35
40
45
50
2θ

Figure 3.

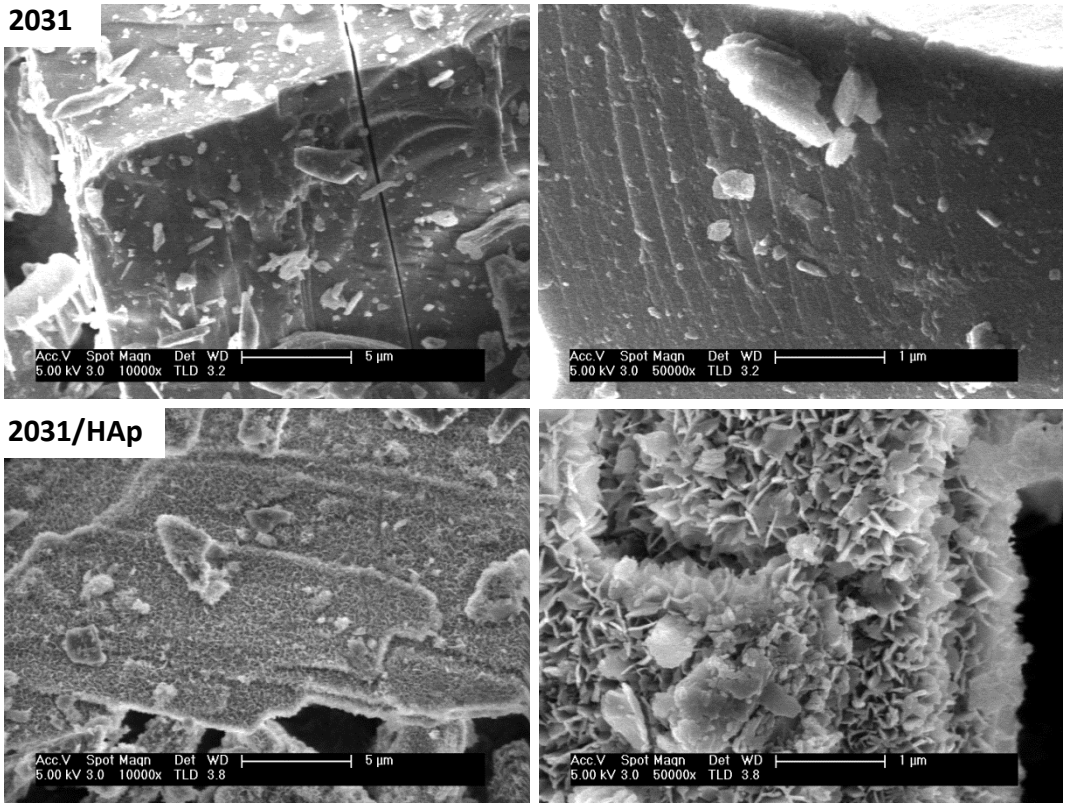
2031
Acc.V Spot Magn Det WD 5 µm
5.00 kV 3.0 10000x TLD 3.2
Acc.V Spot Magn Det WD 1 µm
5.00 kV 3.0 50000x TLD 3.2
2031/HAp
Acc.V Spot Magn Det WD 5 µm
5.00 kV 3.0 10000x TLD 3.8
Acc.V Spot Magn Det WD 1 µm
5.00 kV 3.0 50000x TLD 3.8

Figure 4.

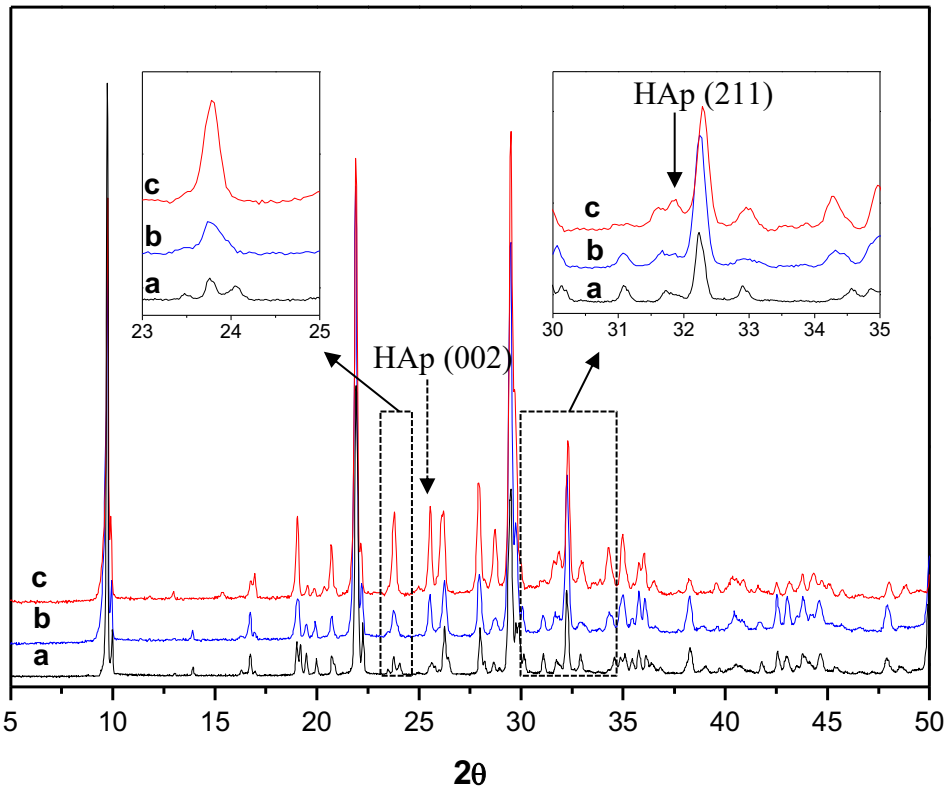
HAp (211)
HAp (002)
c
b
a
23
24
25
30
31
32
33
34
35
5
10
15
20
25
30
35
40
45
50
2θ

Figure 5.

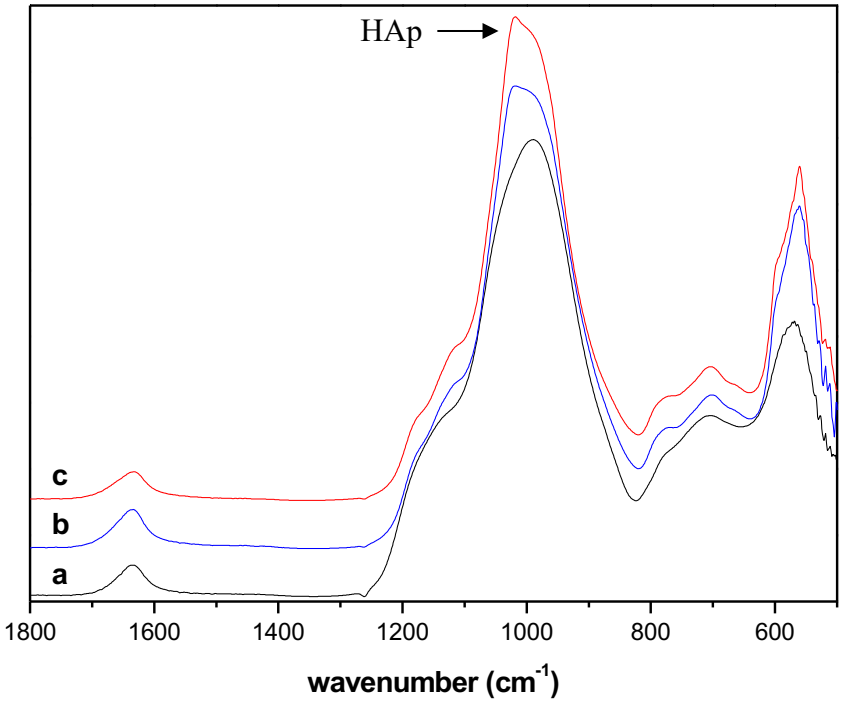

Figure 6.

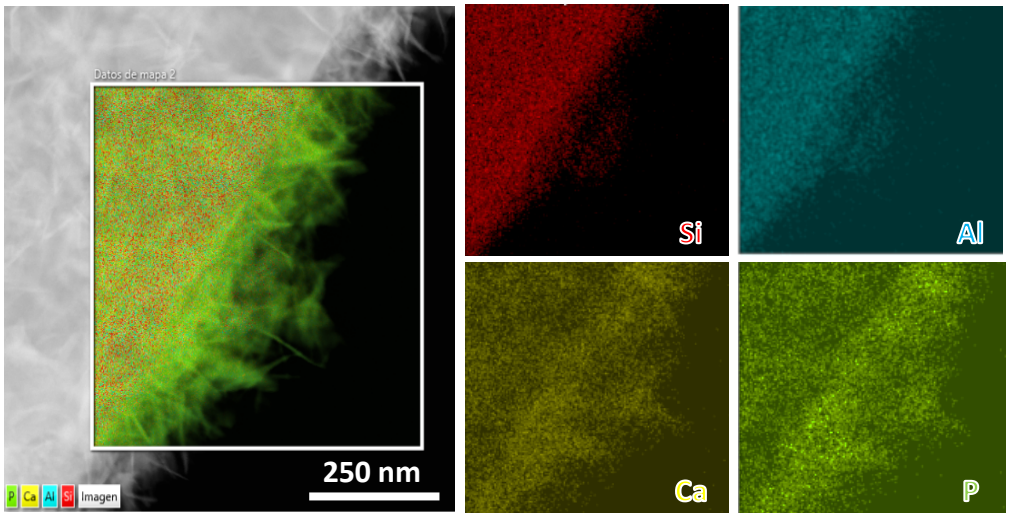

Figure 7.

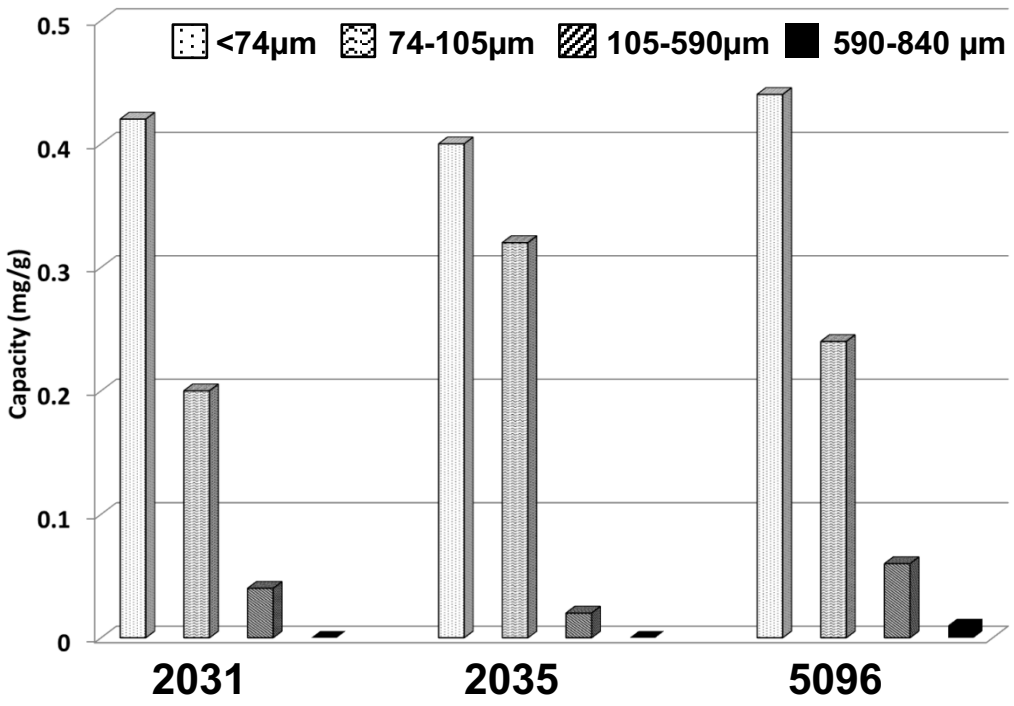
<74µm
74-105µm
105-590µm
590-840 µm
Capacity (mg/g)
0.5
0.4
0.3
0.2
0.1
0
2031
2035
5096

Figure 8.

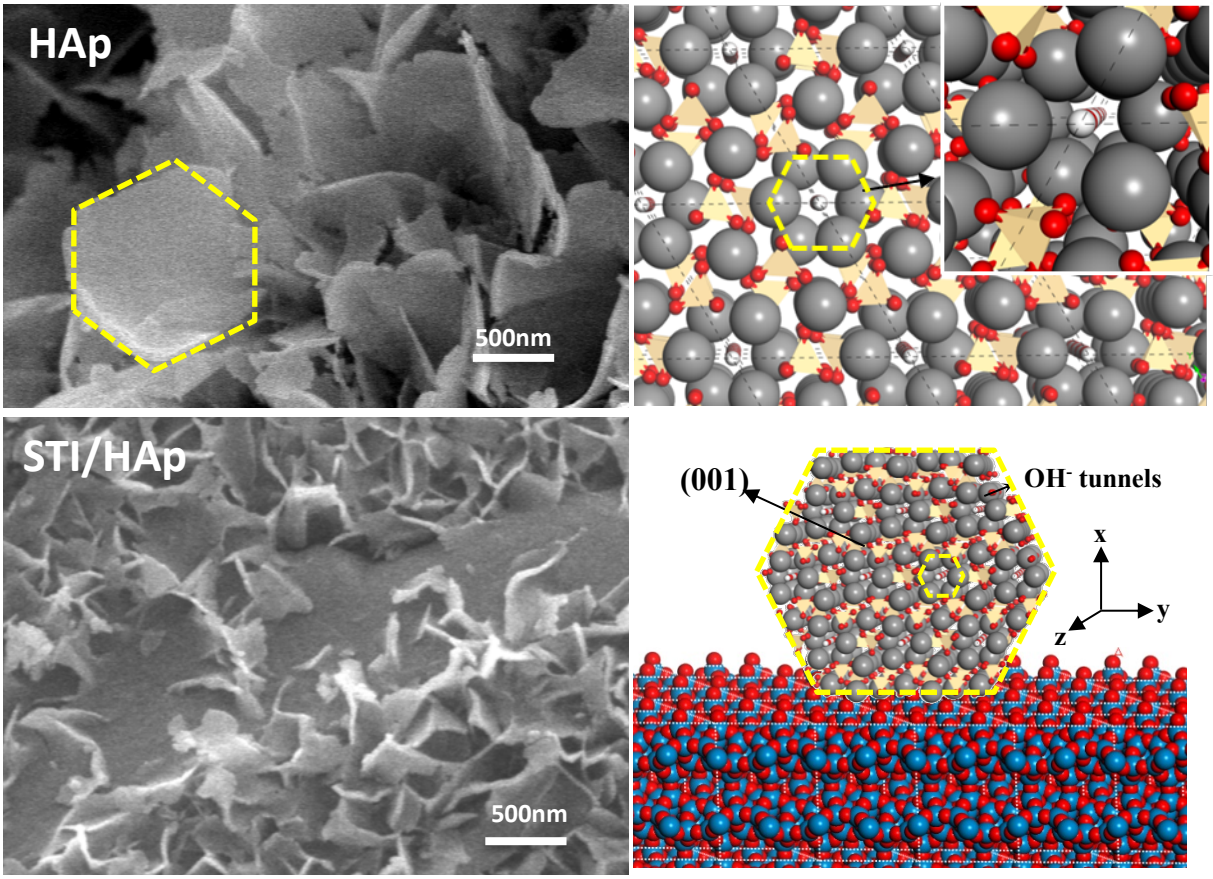

Supplementary Information

Table S1. Chemical composition of the natural water used for the defluoridation tests. Fluoride concentration: 7.3 ppm.

Element	**Concentration (µg/l)**
B	175
Na	464109
Mg	63981
Ca	17209
Al	0
Cr	0
Mn	1.24
Fe	0
Ni	0
Cu	0.29
As	4.64
Se	0
Cd	0.03
Sb	0.25
Hg	0.39
Pb	0
P	123